Malaysian Journal of Mathematical Sciences 14(3): 437–450 (2020)

MALAYSIAN JOURNAL OF MATHEMATICAL SCIENCES

Journal homepage: http://einspem.upm.edu.my/journal

Three-Dimensional Convex and Selective Variational Image Segmentation Model

Jumaat, A. K. *[1] and Chen, K.[2]

[1] *Universiti Teknologi MARA, Malaysia*
[2] *University of Liverpool, United Kingdom*

E-mail: abdulkadir@tmsk.uitm.edu.my
* *Corresponding author*

Received: 30 April 2020
Accepted: 28 August 2020

ABSTRACT

Selective image segmentation is a task of extracting one object of interest among many others in an image based on minimal user input. Several three-dimensional (3-D) selective models were proposed and they would find local minimizer because of their non-convex formulation, hence they are sensitive to initialization. This paper presents a new formulation for 3-D convex selective segmentation model. In order to solve the developed 3-D model, a projection algorithm is proposed. Numerical tests show that the proposed model is effective in segmenting 3-D complex image structures and allowing a global minimizer to be found independently of initialization.

Keywords: Convex segmentation, image processing, level set, selective image segmentation, three dimensional, total variational model

1. Introduction

Variational image segmentation methods based on 2-D level set active contours have been successfully implemented in many applications. These global segmentation methods aim to segment all features or objects in a given image and they may be generalized to 3-D level set active surfaces (Chan and Vese (2002), Huang et al. (2020), Wang et al. (2020), Xie and Mirmehdi (2011), Zhang et al. (2011)). There are some other applications where the selection of one feature among many is required Jumaat et al. (2012a,b), Zaman et al. (2015). This kind of problem leads to a new and challenging task of selective segmentation. Many application fields such as medical imaging and geological surveying can greatly benefit from 3-D selective segmentation, however there exist only a few works for selective segmentation in 3-D.

Some effective selective 3-D segmentation models are Badshah and Chen (2010) that is implemented in Rada and Chen (2014) and 3-D selective model by Rada and Chen (2014). A recent 3-D work by Zhang et al. (2015) applied the narrow band idea of Mille et al. (2009) into Zhang et al. (2014). All the 3-D models mentioned are non-convex, though effective in capturing a local minimizer, is sensitive to initialization where the segmentation result relies heavily on user input.

A 2-D convex selective models is introduced by Spencer and Chen (2015) named convex distance selective segmentation (CDSS), allowing a global minimizer to be found independently of initialization. However, the model is sensitive to regularization and area parameters. A stabilized version of the 2-D model that is less sensitive to the parameters is introduced in Jumaat and Chen (2019). In this paper, we named it as CDSS2 and we will generalize the model by Jumaat and Chen (2019) into 3-D convex formulation. The new 3-D convex formulation is expected to be independent of initialization, hence allowing a global minimizer to be found.

A class of fast algorithm in 2-D framework called Chambolle's projection algorithm by Chambolle (2004) is initially used to solve 2-D image denoising problem and 2-D global image segmentation problem in Bresson et al. (2007). This popular algorithm is considered as powerful (Chan and Chen (2006)) and fast method (Bresson et al. (2007), Chambolle (2004), Chen et al. (2013)). This is mainly because the algorithm able to solve the original convex variational functional (non-differentiable) of image denoising problem without introducing parameter β (to avoid singularity). In 2-D global and convex variational image segmentation problem, the algorithm is used by Chen et al. (2013) to solve a variant of Mumford-Shah model which handles the segmentation of medical

images with intensity inhomogeneities and also in Moreno et al. (2014) for solving a four phase model for segmentation of brain Magnetic Resonance Image (MRI) images by active contours. Due to the strength of the method, we will extend the 2-D Chambolle's projection algorithm in 3-D framework to solve the 3-D convex segmentation model.

In the next section, we will develop our new 3-D convex selective segmentation model and extend the 2-D Chambolle's projection algorithm in 3-D framework. As a benchmark model, we will review the recent 3-D work by Zhang et al. (2015). This is followed by the implementation of our model and the result and discussions of the numerical experiments carried out before we conclude in the last section.

2. Approach and Methods

Recently, we have developed a new stabilised version of 2-D convex selective segmentation model by Spencer and Chen (2015) through primal-dual formulation called CDSS2 in Jumaat and Chen (2019). In 2-D framework, we assume that an image $Z = Z(x, y)$ comprises of two regions of approximately piecewise constant intensities of distinct values (unknown) c_1 and c_2, separated by some (unknown) curve or contour Γ. Let the object to be detected be represented by the region Ω_1 with the value c_1 inside the curve Γ whereas outside Γ, in $\Omega_2 = \Omega \backslash \Omega_1$, the intensity of Z is approximated with value c_2.

In a level set formulation, the unknown curve Γ is represented by the zero level set of the Lipschitz function such that

$$\begin{aligned}
&\Gamma = \{(x, y) \in \Omega : \phi(x, y) = 0\}, \\
&\Omega_1 = \text{inside}(\Gamma) = \{(x, y) \in \Omega : \phi(x, y) > 0\}, \\
&\Omega_2 = \text{outside}(\Gamma) = \{(x, y) \in \Omega : \phi(x, y) < 0\}.
\end{aligned}$$

Let n_1 geometric constraints be given by a marker set

$$A = \{W_i = (x_i^*, y_i^*) \in \Omega, 1 \leq i \leq n_1\} \subset \Omega$$

where each point is near the object boundary Γ, not necessarily on it (Rada and Chen (2013), Zhang et al. (2014)). The selective segmentation idea tries to detect the boundary of a single object among all homogeneity intensity objects in Ω close to A; here $n_1 (\geq 3)$. The geometrical points in A define an initial polygonal contour and guide its evolution towards Γ (Zhang et al. (2014)). Using the set A, construct a polygon Q that connects up the markers. Denote the function $P_d(x, y)$ as the Euclidean distance of each point $(x, y) \in \Omega$ from

its nearest point $(x_p, y_p) \in Q$:

$$P_d(x,y) = \sqrt{(x-x_p)^2 + (y-y_p)^2} = \min_{p \in Q} \|(x,y) - (x_p, y_p)\|$$

Hence, CDSS2 is defined as

$$\min_{u,w \in [0,1]} J(u,w) = \int_\Omega |\nabla u|_g dx + \int_\Omega rw \, dx + \theta \int_\Omega P_d w \, dx + \frac{1}{2\rho} \int_\Omega (u-w)^2 \, dx \tag{1}$$

where ρ and θ are nonnegative parameters, g is an edge detector function used in Badshah and Chen (2010) and Zhang et al. (2015), w is a dual variable and $r = (c_1 - Z)^2 - (c_2 - Z)^2$.

On 3-D plane, an image $Z = Z(x,y,z) = Z(\mathbf{x})$ is defined on the cubic domain Ω. The selective segmentation idea is described as the detection of the boundary of a single target object among all homogeneity intensity object that are defined in a closed domain to the geometrical points in a set $\mathrm{A} = \{W_i = (x_i^*, y_i^*, z_i^*) \in \Omega, 1 \le i \le n_1\} \subset \Omega$, consisting of $n_1 (\ge 3)$ points on or near the target object (Badshah and Chen (2010)). The marker set or the geometrical points in the set A can be used to define an initial solution and to guide its evolution towards Γ. Using the set A, construct a polygon Q that connects up the markers. Denote the function $P_d(\mathbf{x})$ as the Euclidean distance of each point $(\mathbf{x}) \in \Omega$ from its nearest point $(x_p, y_p, z_p) \in Q$:

$$P_d(\mathbf{x}) = \sqrt{(x-x_p)^2 + (y-y_p)^2 + (z-z_p)^2} = \min_{p \in Q} \|(x,y,z) - (x_p, y_p, z_p).\|$$

Thus, the new 3-D convex selective segmentation model i.e the extension of CDSS2 model into 3-D version takes the form

$$\min_{u,w \in [0,1]} J(u,w) = \int_\Omega |\nabla u|_g d\mathbf{x} + \int_\Omega rw \, d\mathbf{x} + \theta \int_\Omega P_d w \, d\mathbf{x} + \frac{1}{2\rho} \int_\Omega (u-w)^2 \, d\mathbf{x}. \tag{2}$$

The unique minimizer of J can be computed by minimising J with respect to u and w separately, iterating the process until convergence as done in Chambolle (2004) and Bresson et al. (2007). In alternating minimization form, the new formulation of equation 2 is equivalent to solve the following functional

$$\min_u \; J_1(u,w) = \int_\Omega |\nabla u|_g d\mathbf{x} + \frac{1}{2\rho} \int_\Omega (u-w)^2 d\mathbf{x}, \tag{3}$$

$$\min_{w\in[0,1]} J_2(u,w) = \int_\Omega rw\, d\mathbf{x} + \theta \int_\Omega P_d w\, d\mathbf{x} + \frac{1}{2\rho}\int_\Omega (u-w)^2\, d\mathbf{x}. \tag{4}$$

The explicit solution of equation 4 is given as

$$w = \min\left\{\max\left\{u(\mathbf{x}) - \rho r - \rho\theta P_d, 0\right\}, 1\right\}. \tag{5}$$

Now it only remains to discuss how to solve equation 3. Next, we propose to extend the Chambolle's projection algorithm (Chambolle (2004)) into 3-D framework to solve our new 3-D selective and convex variational image segmentation problem in equation 3. Again, note that the problem in equation 4 is explicitly solved using equation 5. To develop 3-D Chambolle's method, first define the gradient operator $(\nabla u)_{i,j,k} = \left((\nabla u)^1_{i,j,k}, (\nabla u)^2_{i,j,k}, (\nabla u)^3_{i,j,k}\right)$ where

$$(\nabla u)^1_{i,j,k} = \begin{cases} u_{i+1,j,k} - u_{i,j,k} & \text{if } i < N \\ 0 & \text{if } i = N \end{cases}$$

$$(\nabla u)^2_{i,j,k} = \begin{cases} u_{i,j+1,k} - u_{i,j,k} & \text{if } j < N \\ 0 & \text{if } j = N \end{cases}$$

$$(\nabla u)^3_{i,j,k} = \begin{cases} u_{i,j,k+1} - u_{i,j,k} & \text{if } k < N \\ 0 & \text{if } k = N. \end{cases}$$

The divergence operator:

$$\begin{aligned}(\nabla\cdot p)_{i,j,k} = &\begin{cases} p^1_{i,j,k} - p^1_{i-1,j,k} & \text{if} \quad 1 < i < N \\ p^1_{i,j,k} & \text{if} \quad i = 1 \\ -p^1_{i-1,j,k} & \text{if} \quad i = N \end{cases} \\ &+ \begin{cases} p^2_{i,j,k} - p^2_{i,j-1,k} & \text{if} \quad 1 < j < N \\ p^2_{i,j,k} & \text{if} \quad j = 1 \\ -p^2_{i,j-1,k} & \text{if} \quad j = N \end{cases} \\ &+ \begin{cases} p^3_{i,j,k} - p^3_{i,j,k-1} & \text{if} \quad 1 < k < N \\ p^3_{i,j,k} & \text{if} \quad k = 1 \\ -p^3_{i,j,k-1} & \text{if} \quad k = N. \end{cases}\end{aligned}$$

We proceed exactly as in Chambolle (2004) and Bresson et al. (2007) where equation 3 can be written with the dual variable $p = (p_1, p_2, p_3)$:

$$\min_{u} \max_{|p|\leq g} \int_{\Omega} u\nabla \cdot p + \frac{1}{2\rho}(u-w)^2 d\mathbf{x}. \tag{6}$$

One can now switch the min and max to obtain the equivalent

$$\max_{|p|\leq g} \min_{u} \int_{\Omega} u\nabla \cdot p + \frac{1}{2\rho}(u-w)^2 d\mathbf{x}. \tag{7}$$

The inner minimization in equation 7 is point-wise in u. Carrying it out gives:

$$\nabla \cdot p + \frac{1}{\rho}(u-w) = 0 \Rightarrow u = w - \rho\nabla \cdot p. \tag{8}$$

Substituting the expression equation 8 for minimal u into the $\max - \min$ problem equation 7 gives

$$\max_{|p|\leq g} \int_{\Omega} (w - \rho\nabla \cdot p)\nabla \cdot p + \frac{\rho}{2}(\nabla \cdot p)^2 d\mathbf{x}. \tag{9}$$

Simplifying a bit:

$$\max_{|p|\leq g} \int_{\Omega} w\nabla \cdot p - \frac{\rho}{2}(\nabla \cdot p)^2 d\mathbf{x}. \tag{10}$$

Variation of energy in equation 10 with respect to the vector field p give:

$$\int_{\Omega} (-\nabla w + \rho\nabla(\nabla \cdot p)) \cdot \delta p \, d\mathbf{x}. \tag{11}$$

Along with the point-wise constraint $|p|^2 - g^2 \leq 0$, one gets the optimality condition:

$$-\nabla(\rho\nabla \cdot p - w) + \psi(\mathbf{x})p = 0 \tag{12}$$

where the Lagrange multiplier $\psi(\mathbf{x}) \geq 0$ for all $\mathbf{x}$. As Chambolle shows in Chambolle (2004), it can be determined and eliminated as follows: if the constraint is not active at a point $\mathbf{x}$, that is if $|p(\mathbf{x})|^2 < g^2(\mathbf{x})$, then $\psi(\mathbf{x}) = 0$. Otherwise, if the constraint is active at a point $\mathbf{x}$, that is, if $|p(\mathbf{x})|^2 = g^2(\mathbf{x})$, then

$$|\nabla(\rho\nabla\cdot p - w)|^2 - \psi^2 g^2(\mathbf{x}) = 0 \tag{13}$$

which leads to the conclusion that in either case, the value of $\psi(\mathbf{x})$ is given by:

$$\psi = \frac{1}{g(\mathbf{x})}|\nabla(\rho\nabla\cdot p - w)|. \tag{14}$$

Substituting equation 14 into equation 12 gives:

$$-\nabla(\rho\nabla\cdot p - w) + \frac{1}{g(\mathbf{x})}|\nabla(\rho\nabla\cdot p - w)|\, p = 0. \tag{15}$$

We can use a semi-implicit gradient descent algorithm, as proposed by Chambolle in Chambolle (2004), to solve equation 15 as

$$p^{n+1} = \frac{p^n + \delta t\nabla(\nabla\cdot p^n - w/\rho)}{1 + \frac{\delta t}{g(\mathbf{x})}|\nabla(\nabla\cdot p^n - w/\rho)|}. \tag{16}$$

Thus, the solution for equation 3 is updated using the following equation

$$u = w - \rho\nabla\cdot p. \tag{17}$$

We call the 3-D Chambolle's projection algorithm to solve our 3-D convex and selective segmentation problem as 3DA. The overall procedure to solve the 3-D model is given below.

3DA– Algorithm to solve the new 3-D model:- *Given input image Z, an initial guess u^0, initial $p^0 = 0$, θ, ρ and the stop tolerance (tol). Compute c_1, c_2 and P_d. Set $w^0 = u^0$.*

1. *Update p^{n+1} using equation* 16.
2. *Update u^{n+1} using equation 17.*
3. *Solve equation 5 to update w.*
4. *Check the stopping criteria:* $\max\left(\frac{\|u^{n+1}-u^n\|}{\|u^n\|}, \frac{\|w^{n+1}-w^n\|}{\|w^n\|}\right) < tol$. *If not satisfied, return to Step 1. Otherwise exit with solution u and w.*

The most recent 3-D non- convex selective segmentation model is formulated by Zhang et al. (2015) that takes the form

$$\min_{\Gamma, c_1, c_2} \left\{ E\left(\Gamma, c_1, c_2\right) = \mu E_G\left(\Gamma\right) + E_F\left(\Gamma, c_1, c_2\right) \right\} \tag{18}$$

where $E_G\left(\Gamma\right) = \int_\Gamma G\left(\mathbf{x}\right) ds$ with $G\left(\mathbf{x}\right) = g\left(\mathbf{x}\right) d\left(\mathbf{x}\right)$. Here the function $g\left(\mathbf{x}\right) = \frac{1}{1+q\left|\nabla z(\mathbf{x})\right|^2}$ is an edge detector function which helps to stop the evolving curve on the edge of the targeted object in an image. The function $d\left(\mathbf{x}\right)$ is a marker distance function, which is close to 0 when approaching the points from marker set A given as:

$$d\left(\mathbf{x}\right) = \text{distance}\left(\left(\mathbf{x}\right), \mathrm{A}\right) = \prod_{i=1}^{n_1} \left(1 - e^{-\frac{\left(\mathbf{x} - \overset{*}{i}\right)^2}{2\kappa^2}}\right), \quad \forall\left(\mathbf{x}\right) \in \Omega$$

where κ is a positive constant. Alternative distance functions $d\left(\mathbf{x}\right)$ are also possible (Zhang et al. (2015)). The new local fitting energy $E_F\left(\Gamma, c_1, c_2\right)$ is

$$\left\{ \lambda_1 \int_{\Omega_{in}(\Gamma)} b_1\left(\phi\left(\mathbf{x}\right), \gamma_{in}\right) \left(z\left(\mathbf{x}\right) - c_1\right)^2 d\mathbf{x} + \lambda_2 \int_{\Omega_{out}(\Gamma)} b_2\left(\phi\left(\mathbf{x}\right), \gamma_{out}\right) \left(z\left(\mathbf{x}\right) - c_2\right)^2 d\mathbf{x} \right\}$$

where $b_1\left(\phi\left(\mathbf{x}\right), \gamma_{in}\right) = B\left(\phi\left(\mathbf{x}\right), \gamma_{in}, 0\right)$ and $b_2\left(\phi\left(\mathbf{x}\right), \gamma_{out}\right) = B\left(\phi\left(\mathbf{x}\right), 0, \gamma_{out}\right)$ with

$$B\left(\phi\left(\mathbf{x}\right), \gamma_{in}, \gamma_{out}\right) = H\left(\phi\left(\mathbf{x}\right) + \gamma_{in}\right)\left(1 - H\left(\phi\left(\mathbf{x}\right) - \gamma_{out}\right)\right) \tag{19}$$

where H is a heaviside function. In the numerical experiment, we will consider the model by Zhang et al. (2015) as a comparison to our new model.

3. Implementation

There are two sets of tests carried out. In the first set, we will test the performance of 3DA in segmenting one synthetic image and one medical image. In the second set, we will compare the performance of 3DA with a recent 3-D selective segmentation model by Zhang et al. (2015), called 3DB in terms of sensitivity to different initializations in segmenting a real medical image.

For synthetic image, the segmentation quality is measured based on the Jaccard similarity coefficient (JSC):

$$JSC = \frac{|S_n \cap S_*|}{|S_n \cup S_*|}$$

where S_n is the set of the segmented domain u and S_* is the true set of u (which is only easy to obtain for simple images). The similarity functions return values in the range $[0, 1]$. The value 1 indicates perfect segmentation quality while the value 0 indicates poor quality. The segmentation quality for real medical images is measured visually since we don't have true solution in hand.

Figure 1(a) and (b) shows the image used in test set 1 of size $128 \times 128 \times 128$, while the images in Figure 1(c) and (d) of size $256 \times 256 \times 256$ are used in test set 2. The markers set are in red and the green polyhedral surface constructed based on the position of markers set are the initial solution. All algorithms are implemented in MATLAB R2019a on a laptop with Intel Core i5 processor, CPU 2.5GHz, 8 GB RAM CPU and stop when they reach $tol = 10^{-4}$. The parameter $\rho = 10^{-3}$ and $\delta t = 10^{-2}$. Tuning the parameter θ depends on the targeted object. If the object is too close to a nearby boundary then θ should be large. Segmenting a clearly separated object in an image needs just a small θ.

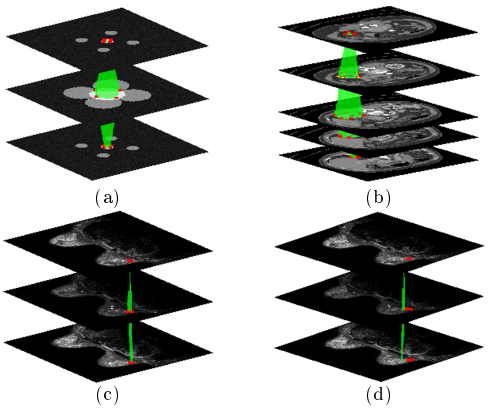

Figure 1: (a) and (b) are images used in test set 1 while (c) and (d) for test set 2. Markers set are in red and the green polyhedral surface constructed based on the position of markers set are the initial solution.

4. Result and Discussion

In this section, both test sets will be discussed.

4.1 Test Set 1: Segmentation performance of 3DA

In the first experiment, we will segment images in Fig. 1(a) and (b) using the 3DA. For the synthetic image in Fig. 1(a), we used $\theta = 4000$ while $\theta = 11000$ for the real medical image (kidney) in Fig. 1(b). Figure 2(a) demonstrates the successful segmentation results for the 3DA in segmenting simple (synthetic) image. The JSC value for image in Fig. 2(a) is 1.0 which indicates a high value of accuracy. In Figure 2(b), it is shown that the 3DA successful in segmenting complex (medical) type of image. Since we don't have true solution in hand, there is no JSC value computed for the result, hence the segmentation quality for the real medical image is measured visually.

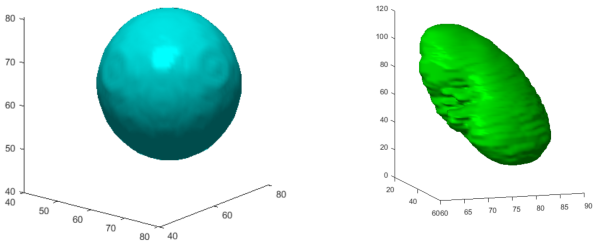

(a) (b)

Figure 2: Successful segmentation result for 3DA in segmenting synthetic and medical images in (a) and (b) respectively.

4.2 Test Set 2: Comparison of 3DA with 3DB (Zhang et al. (2015))

Finally, we compare the performance of the 3DA with 3DB (Zhang et al. (2015)) in segmenting MRI medical data that contains breast disease using different initialization. The segmentation quality for this real medical image is measured visually since we don't have true solution in hand. Here $\theta = 2 \times 10^4$. Figure 3(a) shows the data with initial solution constructed based on the location of marker points while Figure 3(b) shows the initial solution is located slightly away from the marker. Figure 3 1(a) and 2(a) illustrate the success-

ful result by 3DB and 3DA respectively using initial solution in Figure 3(a). For the second initialization in 3(b), the 3DA gives a consistent segmentation curve as shown in Figure 3 2(b), showing the advantages of our convex formulation model. However, the segmentation results of 3DB are inconsistent which implies that 3DB is heavily dependent on the initilization due to highly non-convex terms involve in the minimization problem.

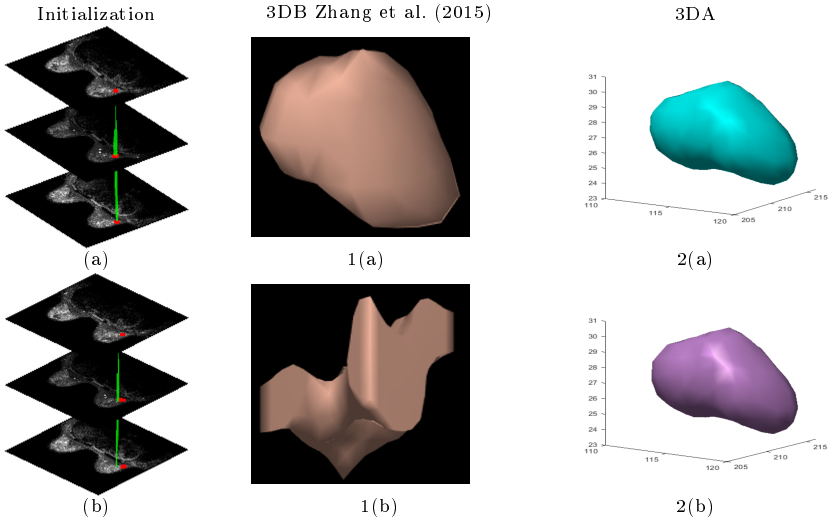

Figure 3: Test Set 2–Segmentation performance of 3DB and 3DA using 2 different initializations. With initialization 1 in (a), the segmentation results for 3DB and 3DA are illustrated in 1(a) and 2(a) respectively. With initialization 2 in (b), the segmentation results for 3DB and 3DA are illustrated in 1(b) and 2(b) respectively. Clearly, our model 3DA gives a consistent segmentation result indicating that our model is less dependent on initialization while 3DB is sensitive to initialization as indicated by different results obtained

5. Conclusion

In this paper, we have successfully developed a 3-D convex and selective segmentation model and solved using the extension of Chambolle's projection algorithm in 3-D framework and name it as 3DA. Experiments carried on synthetic image show that 3DA gives successful result with high accuracy value indicated by the JSC value. The comparison of 3DA with a recent 3-D selective segmentation model called 3DB is also conducted. Results show the 3DA is consistent with different initial solution (less dependent of initialization) compare to 3DB which is sensitive to initial solution. These findings demonstrate the effectiveness of convex formulation over the non-convex formulation segmentation model. In future work, we will consider to extend the multilevel

solver by Jumaat and Chen (2017) in 3-D framework in order to solve our model in segmenting large image size.

Acknowledgement

The first author would like to thank to Faculty of Computer and Mathematical Sciences, Universiti Teknologi MARA Shah Alam and Ministry of Higher Education of Malaysia for funding a scholarship to support this research. The second author is grateful to the support from the UK EPSRC for the grant EP/N014499/1.

References

Badshah, N. and Chen, K. (2010). Image selective segmentation under geometrical constraints using an active contour approach. *Communications in Computational Physics*, 7(4):759–778.

Bresson, X., Esedoglu, S., Vandergheynst, P., thiran, J. P., and Osher, S. (2007). Fast global minimization of the active contour/snake model. *Journal of Mathematical Imaging Vision*, 28:151–167.

Chambolle, A. (2004). An algorithm for total variation minimization and applications. *Journal of Mathematical Imaging and Vision*, 20(1-2):89–97.

Chan, T. and Vese, L. A. (2002). *Active Contour and Segmentation Models using Geometric PDEs for Medical Imaging. In: Malladi R. (eds) Geometric Methods in Bio-Medical Image Processing. Mathematics and Visualization.* Berlin, Heidelberg: Springer.

Chan, T. F. and Chen, K. (2006). An optimization-based multilevel algorithm for total variation image denoising. *Multiscale Modelelling and Simullation*, 5(2):615–645.

Chen, D., Yang, M., and Cohen, L. D. (2013). Global minimum for a variant mumford-shah model with application to medical image segmentation. *Computer Methods in Biomechanics and Biomedical Engineering: Imaging and Visualization*, 1(1):48–60.

Huang, B., Pan, Z., Yang, H., and Bai, L. (2020). Variational level set method for image segmentation with simplex constraint of landmarks. *Signal Processing: Image Communication*, 82:1–12.

Jumaat, A. K. and Chen, K. (2017). An optimization-based multilevel algorithm for variational image segmentation models. *Electronic Transactions on Numerical Analysis*, 46:474–504.

Jumaat, A. K. and Chen, K. (2019). A reformulated convex and selective variational image segmentation model and its fast multilevel algorithm. *Numerical Mathematics: Theory, Methods and Applications*, 12:403–437.

Jumaat, A. K., Rahman, W. E. Z. W. A., Ibrahim, A., Yasiran, S. S., and Mahmud, R. (2012a). Masses characterization using active contour. *Journal of Communication and Computer*, 9:1358–1363.

Jumaat, A. K., Rahman, W. E. Z. W. A., Yasiran, S. S., Mahmud, R., and Malek, A. (2012b). Masses characterization based on angular margin measurement. In *Fourth International Conference on Computational Intelligence, Modelling and Simulation*, pages 265–269. http://doi.org/10.1109/CIMSim.2012.50.

Mille, J., Bone, R., P.Makris, and Cardot, H. (2009). Narrow band region-based active contours and surfaces for 2d and 3d segmentation. *Computer Vision and Image Understanding*, 113:946–965.

Moreno, J. C., Prasath, V. B. S., Proenca, H., and Palaniappan, K. (2014). Fast and globally convex multiphase active contours for brain mri. *Computer Vision and Image Understanding*, 125:237–250.

Rada, L. and Chen, K. (2013). Improved selective segmentation model using one level set. *Journal of Algorithm and Computational Technology*, 7:509–541.

Rada, L. and Chen, K. (2014). A variational model and its numerical solution for local, selective and automatic segmentation. *Numerical Algorithm*, 66:399–430.

Spencer, J. and Chen, K. (2015). A convex and selective variational model for image segmentation. *Communication in Mathematical Sciences*, 13:1453–1452.

Wang, L., Zhang, L., Yang, X., Yi, P., and Chen, H. (2020). Level set based segmentation using local fitted images and inhomogeneity entropy. *Signal Processing*, 167:1–8.

Xie, X. and Mirmehdi, M. (2011). Radial basis function based level set interpolation and evolution for deformable modelling. *Image Vision and Computing*, 29:167–177.

Zaman, N. A. K., Rahman, W. E. Z. W. A., Jumaat, A. K., and Yasiran, S. S. (2015). Classification of breast abnormalities using artificial neural network. In *AIP Conference Proceedings*, page 050038. https://doi.org/10.1063/1.4915671.

Zhang, J., Chen, K., and Gould, D. (2015). A fast algorithm for automatic segmentation and extraction of a single object by active surfaces. *International Journal of Computer Mathematics*, 92:1251–1274.

Zhang, J., Chen, K., and Yu, B. (2011). A multigrid algorithm for the 3d chan-vese model of variational image segmentation. *International Journal of Computer Mathematics*, 89:160–189.

Zhang, J., Chen, K., Yu, B., and Gould, D. (2014). A local information based variational model for selective image segmentation. *Journal of Inverse Problems and Imaging*, 8:293–320.